LEMONY – a library of empirical medium-resolution spectra by observations with the NAOC Xinglong 2.16-m and YNAO Gaomeigu 2.4-m telescopes

C. Wang [1]★ X-W. Liu,[1,2]★ Y. Huang,[1,2]† M-S. Xiang,[3]† J-J. Ren,[3] H-B. Yuan,[4] B-Q. Chen,[2]† Z-J. Tian,[1]† J-M. Bai,[5] N-C. Sun,[1] F. Zuo,[3] H-W. Zhang,[1] Y-W. Zhang,[5] Z. Fan,[3] A-L. Luo [3] J-R. Shi,[3] J. Li[6] and Y-L. Shao[1]

[1]*Department of Astronomy, Peking University, Beijing 100871, China*
[2]*South-Western Institute for Astronomy Research, Yunnan University, Kunming, Yunnan 650091, China*
[3]*National Astronomical Observatories, Chinese Academy of Sciences, Beijing 100012, China*
[4]*Department of Astronomy, Beijing Normal University, Beijing 100875, China*
[5]*Yunnan Observatories, Chinese Academy of Sciences, Kunming, Yunnan 650011, China*
[6]*Department of Space Science and Astronomy, Hebei Normal University, Shijiazhuang 050024, China*

ABSTRACT

In this study, we expand the coverage and improve the homogeneity of the distribution of MILES template stars in the parameter space, as well as extend the wavelength coverage of the template spectra to the far red beyond the Ca II triplet. To achieve this, we have carried out a major observational campaign using two long-slit spectrographs: the OMR mounted on the National Astronomy Observatory of China (NAOC) 2.16-m telescope and the Yunnan Faint Object Spectrograph and Camera (YFOSC) mounted on the Yunnan Astronomical Observatory (YNAO) 2.4-m telescope. The original sample is based on the MILES library, supplemented by 918 stars selected from the PASTEL data base. In total, 822 OMR and 1324 YFOSC spectra have been collected and reduced, covering the wavelength ranges $\lambda\lambda3800$–5180 and $\lambda\lambda5150$–9000, respectively. The spectra have a mean resolution full width at half-maximum of ~3.3 Å and are wavelength- and flux-calibrated to an accuracy of ~20 km s^{-1} and ~5 per cent, respectively. The spectra are further corrected for systematic errors in the wavelength calibration to an accuracy of ~4 km s^{-1} by cross-correlating with the theoretical spectra. Almost all the spectra have an average signal-to-noise ratio better than 100 per pixel. Combined with the MILES spectra, there are now 1731, 1542, 1324 and 1273 stars with spectra covering $\lambda\lambda3800$–5180, $\lambda\lambda3800$–7500, $\lambda\lambda5150$–9000 and $\lambda\lambda3800$–9000, respectively. In this paper, we describe our template star selection, the observation and data reduction, and we present the reduced spectra collected hitherto.

Key words: techniques: imaging spectroscopy – stars: fundamental parameters.

1 INTRODUCTION

A low- to medium-resolution spectral library with a good and homogeneous coverage of the stellar atmospheric parameter space (i.e. effective temperature T_{eff}, surface gravity log g and metallicity [Fe/H]) is an important tool in many astronomical applications, from the spectral synthesis analyses of stellar populations of galaxies (Guiderdoni & Rocca-Volmerange 1987; Buzzoni 1989; Worthey 1994; Leitherer et al. 1996; Vazdekis 1999; Bruzual & Charlot 2003; Leitherer et al. 2010; Vazdekis et al. 2012; Milone et al. 2014; Röck et al. 2016) to the determination of stellar atmospheric parameters using spectral template matching (Adelman-McCarthy et al. 2008; Lee et al. 2008; Boeche et al. 2011; Wu et al. 2011; Xiang et al. 2015). The latter has become increasingly important, driven by a number of already completed or still ongoing large-scale spectroscopic surveys, such as the Sloan Extension for Galactic Understanding and Exploration (SEGUE; Yanny et al. 2009), the Radial Velocity Experiment (RAVE; Steinmetz et al. 2006), the Large sky Area Multi-Object fiber Spectroscopic Telescope (LAMOST) Galactic Spectroscopic Surveys (Deng et al. 2012; Zhao et al. 2012;

★ E-mail: wchun@pku.edu.cn (CW); x.liu@pku.edu.cn (XWL)
† LAMOST Fellow.

Liu et al. 2014; Yuan et al. 2015), and the APO Galactic Evolution Experiment (APOGEE; Majewski 2012). These surveys are providing huge amounts of low- to intermediate-resolution spectral data to help improve our understanding of the structure, kinematics and chemistry, and formation and evolution of our Galaxy – the Milky Way – and of other galaxies in general.

Specifically, the ongoing LAMOST Galactic Spectroscopic Surveys have hitherto collected over 7.5 million low-resolution ($R \sim$ 1800) quality optical spectra (Liu, Zhao & Hou 2015). To derive robust estimates of the stellar atmospheric parameters as well as the radial velocities from this huge data set, two stellar parameter determination pipelines based on the technique of spectral template matching have been developed: the LAMOST Stellar Parameter Pipeline (LASP; Luo et al. 2015) and the LAMOST Stellar Parameter Pipeline at Peking University (LSP3; Xiang et al. 2015). LASP determines both the atmospheric parameters as well as the radial velocities by template matching with the empirical spectral library ELODIE (Prugniel & Soubiran 2001), whereas LSP3 uses ELODIE for the radial velocity determinations and another empirical spectral library, MILES (Sánchez-Blázquez et al. 2006; Falcón-Barroso et al. 2011), for the atmospheric parameter determinations.

Several other empirical (Jones 1999; Cenarro et al. 2001; Le Borgne et al. 2003; Valdes et al. 2004; Sánchez-Blázquez et al. 2006; Heap & Lindler 2007; Falcón-Barroso et al. 2011; Vazdekis et al. 2012; Chen et al. 2014) or synthetic (Lastennet et al. 2002; Barbuy et al. 2003; Murphy & Meiksin 2004; Coelho et al. 2005; Martins et al. 2005; Munari et al. 2005a) spectral libraries are now available (see the recent review by Wu et al. 2011). Compared to synthetic spectra, empirical spectra have the advantage that they represent *real* stars. However, empirical spectral libraries are always restricted by the available observations and thus limited in terms of the parameter space coverage (Martins & Coelho 2007; Wu et al. 2011). Because of either the lack of a wide coverage of the stellar atmospheric parameter space or insufficiently accurate flux-calibration over a wide wavelength range, most of these currently available empirical spectral libraries are not suitable as template spectral libraries for the determinations of stellar atmospheric parameters. For example, STELIB (Le Borgne et al. 2003), NGSL (Heap & Lindler 2007), XSL (Chen et al. 2014) and the Extended IRTF Library (Villaume et al. 2017) have insufficient atmospheric parameter space coverage, while INDO-US (Valdes et al. 2004) and MIUSCAT (Vazdekis et al. 2012) suffer from poor flux-calibration, and CaT (Cenarro et al. 2001) and Jones (Jones 1999) have narrow wavelength coverages. In comparison, MILES and ELODIE, adopted as the template library for LASP and LSP3, respectively, have broad atmospheric parameter coverages as well as wide wavelength ranges. MILES spectra were observed using a long-slit spectrograph with a spectral resolution comparable to that of the LAMOST spectra and were accurately flux-calibrated to a few per cent (Sánchez-Blázquez et al. 2006). In comparison, ELODIE spectra were obtained by the ELODIE spectrograph with medium ($R \sim 10\,000$) to high ($R \sim 42\,000$) spectral resolution and were poorly flux-calibrated. Thus, the MILES spectral library is ideal for the determinations of atmospheric parameters, although ELODIE works much better for radial velocity determinations, given the much higher spectral resolution of the spectra of the latter (Xiang et al. 2015). With MILES, LSP3 has achieved a precision of 150 K, 0.25 dex and 0.15 dex for the determinations of $T_{\rm eff}$, $\log g$ and [Fe/H], respectively, for LAMOST spectra of FGK-type stars with signal-to-noise (S/N) ratios per pixel better than 10.

As discussed in Xiang et al. (2015) and Yuan et al. (2015), there are several aspects of the MILES library that need further improvement. First, while the library has a decent coverage of the stellar parameter space, the distribution of stars in the parameter space is not uniform – there are clusters and holes of stars in the distribution that produce systematic errors in the derived atmospheric stellar parameters (Xiang et al. 2015). A more acute problem is that the spectra only cover wavelength ranges up to 7500 Å. Given that the LAMOST Galactic Spectroscopic Surveys target stars of all colours in the Galactic disc and halo, there is a significant fraction (about 30 per cent) of spectra that meet the survey S/N ratio requirement (i.e. better than 10) in the red, but fail to do so in the blue, either because the stars are intrinsically red (i.e. of late spectral types) or heavily reddened by the interstellar dust grains, or both. The lack of suitable template spectra in the red is largely responsible for the fact that of all the spectra hitherto collected by LAMOST, only just over half have the atmospheric parameters determined (Luo et al. 2015; Yuan et al. 2015). Although there are several empirical libraries (e.g. MIUSCAT, INDO-US, STELIB, NGSL, XSL and the Extended IRTF Library as mentioned above) that provide spectra covering almost the whole optical wavelength range, those spectra are either poorly flux-calibrated or have insufficient coverage of the atmospheric parameter space. Thus, it is highly desirable to extend the wavelength coverage of all MILES template spectra to the far red, beyond the Ca II triplet for example. Finally, there is also room for expansion in the parameter coverage of MILES template stars, particularly toward low metallicities and low effective temperatures. With the above considerations in mind, we have embarked on a massive campaign to expand the MILES empirical spectral library. To maintain the maximum internal consistency, all spectra will be collected using long-slit spectrographs with a spectral resolution comparable to that of the MILES spectra and accurately flux-calibrated to a few per cent. Additional template stars with accurately known atmospheric parameters, mostly determined with high-resolution spectroscopy, are selected and added to the library, and observed in order to increase the parameter coverage as well as to improve the homogeneity of the distribution of template stars in the parameter space. Spectra extending to the far red will also be collected such that the LAMOST spectra of stars of either intrinsically red colours or heavily reddened by dust grains can also be properly analysed with LSP3. The spectra collected will also be of interest for other applications such as the spectral synthesis analyses of stellar populations of galaxies, as mentioned above.

The observed spectra with high S/N ratios (better than 100 per pixel) collected in LEMONY – a library of empirical medium-resolution spectra by observations with the NAOC Xinglong 2.16-m and YNAO Gaomeigu 2.4-m telescopes – are accurately wavelength- and flux-calibrated, and cover almost the whole optical range of $\lambda\lambda$ 3800–9000 at a full width at half-maximum (FWHM) resolution of $\sim$3.3 Å. The spectra were collected with the NAOC 2.16-m telescope in the blue and with the YNAO 2.4-m telescope in the red.

Here we present the final results of this observational campaign. The paper is organized as follows. In Section 2, we describe the selection of additional template stars and observations. The data reduction is presented in Section 3. We describe the new library LEMONY as a guide for its use in Section 4. Qualities of the secured spectra are examined and discussed in Section 5. In Section 6, we discuss some improvements of LSP3 based on LEMONY. Finally, in Section 7, we summarize the main results of the paper.
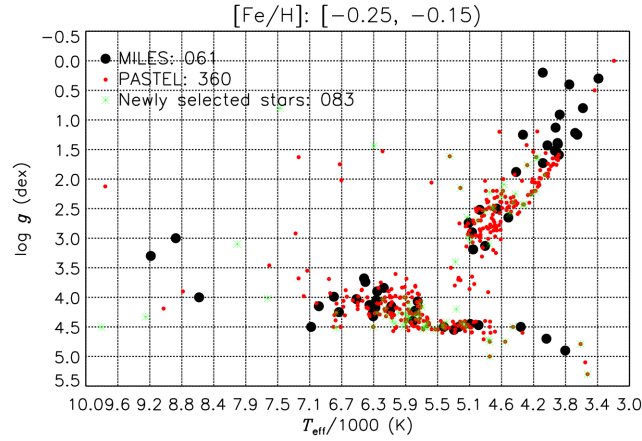
Figure 1. Selecting new template stars for the metallicity bin $-0.25 \leq$ [Fe/H] < -0.15 dex. Stars from the MILES library, from the PASTEL catalogue and those newly selected stars are marked by large black dots, small red dots and small green starry dots, respectively.

Table 1. Metallicity bins used to select new template stars, and the numbers of MILES stars and the newly added template stars in the individual bins.

[Fe/H] metallicity bin (dex)	[−5.0,−1.75)	[−1.75,−1.25)	[−1.25,−1.0)	[−1.0,−0.75)	[−0.75,−0.65)
Number of stars in MILES	44	71	35	64	34
Number of newly added stars	33	37	20	37	16
[Fe/H] metallicity bin (dex)	[−0.65,−0.55)	[−0.55,−0.45)	[−0.45,−0.35)	[−0.35,−0.25)	[−0.25,−0.15)
Number of stars in MILES	33	44	43	75	66
Number of newly added stars	23	33	61	50	83
[Fe/H] metallicity bin (dex)	[−0.15,−0.05)	[−0.05,0.05)	[0.05,0.15)	[0.15,0.25)	[0.25,1]
Number of stars in MILES	72	105	104	46	79
Number of newly added stars	126	148	103	76	72
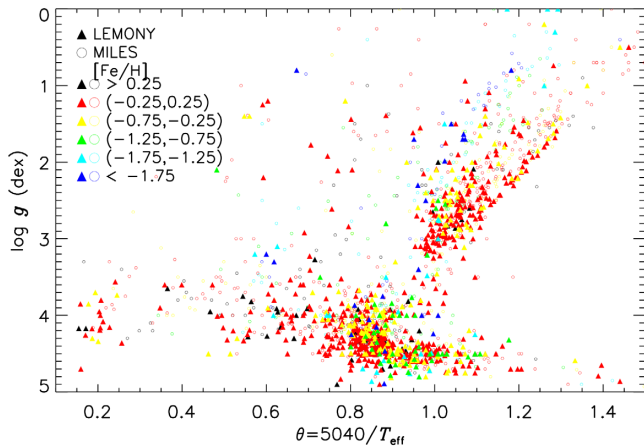
**Figure 2.** Distribution of template stars in the LEMONY library in the T_{eff}−log g plane. Different symbols are used for stars from the MILES library and for newly added stars, whereas different colours are used to indicate stars in different metallicity bins, as marked in the top-left corner of the diagram.

2 OBSERVATIONS

2.1 Target selection

As described above, the observational campaign to provide a new stellar library has two goals: to increase the coverage in comparison to the MILES library and to improve the homogeneity of the distribution of the template stars in the parameter space. For this purpose, we have selected 918 additional template stars from the PASTEL (Soubiran et al. 2010) catalogue, a bibliographical compilation of accurate stellar atmospheric parameters including T_{eff}, log g and [Fe/H], mostly determined with high-resolution, high-S/N spectra. By 2013, the catalogue contained 18 096 atmospheric parameter measurements for 8428 unique stars, collected from 865 bibliographical references. For a given star, if one of the parameters has more than one determination, the average is adopted for that parameter after 3σ-clipping. However, the adoption of the simple averages of measurements available in the literature might lead to some systematic errors, as the values collected from different sources do not always have the same quality and are often determined using different techniques. Also, note that not all values of effective temperature and surface gravity listed in PASTEL were determined with high-resolution spectra. To solve this problem, we have recalibrated the measurements of stellar atmospheric parameters collected in PASTEL (which includes essentially all stars in the MILES library) from a variety of sources such that they are on the same scale. The effective temperatures are recalibrated using the empirical metallicity-dependent calibrations of effective temperature against colours presented by Huang et al. (2015). The surface gravities are directly derived from the stellar radii and masses. The stellar radii are determined using the *Hipparcos* (Perryman et al. 1997) distances and the effective temperatures. The stellar masses are determined from the stellar evolution models based on the measured stellar luminosities, effective temperatures and metallicities. The metallicities are recalibrated using 34 benchmark stars of different spectral types, with measured metallicities accurate to better than 0.02 dex (Jofré et al. 2015).
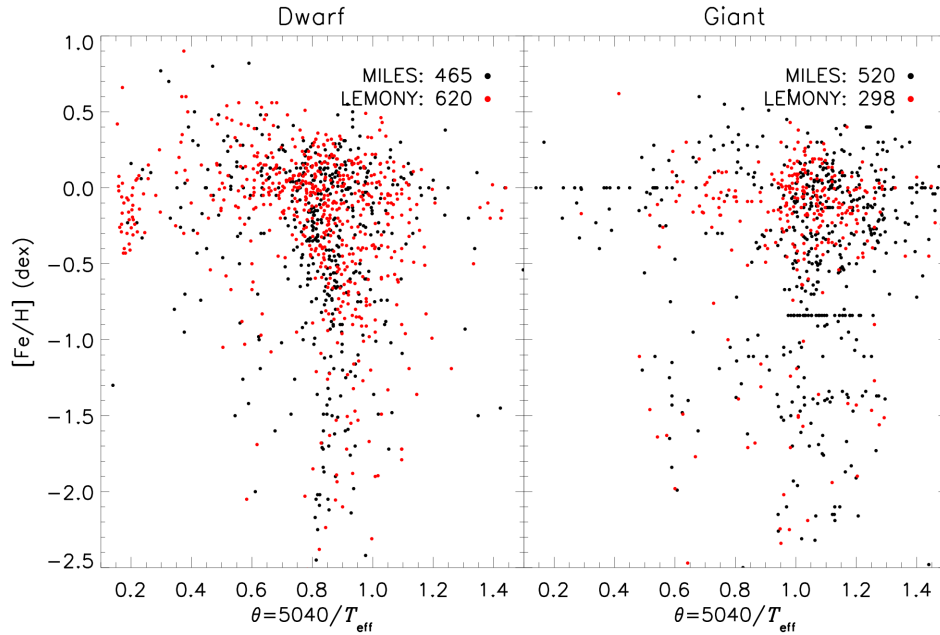
Figure 3. Same as Fig. 2 but in the $T_{\rm eff}$–[Fe/H] plane. Also, dwarfs (log g > 3.5 dex; left panel) and giants (log g ≤ 3.5 dex; right panel) are plotted separately. Black and red dots denote stars from the MILES library and the newly added stars, respectively.

Table 2. Spectrophotometric standard stars used in the current campaign (see http://www.eso.org/sci/observing/tools/standards/spectra/stanlis.html).

Star	RA (J2000.0) hh:mm:ss	Dec. (J2000.0) dd:mm:ss	V (mag)	Spectral type
HR 153	00:36:58.30	+53:53:48.9	3.66	B2 IV
HR 718	02:28:09.54	+08:27:36.2	4.28	B9 III
HR 1544	04:50:36.69	+08:54:00.7	4.36	A1 V
G191–B2B	05:05:30.62	+52:49:54.0	11.78	DA 1
BD+75d325	08:10:49.31	+74:57:57.5	9.54	O5p
HR 3454	08:43:13.46	+03:23:55.1	4.3	B3V
Feige34	10:39:36.71	+43:06:10.1	11.18	DO
HD 93521	10:48:23.51	+37:34:12.8	7.04	O9 Vp
HR 4468	11:36:40.91	−09:48:08.2	4.7	B9.5V
Feige56	12:06:47.3	+11:40:13	11.06	B5p
Feige66	12:37:23.55	+25:04:00.3	10.50	sd0
HR 4936	13:09:56.96	−05:32:20.5	4.38	A1 IV
HR 5501	14:45:30.25	+00:43:02.7	5.68	B9.5 V
BD+33d2642	15:51:59.86	+32:56:54.8	10.81	B2 IV
HR 7001	18:36:56.33	+38:47:01.1	0.00	A0 V
HR 7596	19:54:44.80	+00:16:24.6	5.62	A0 III
HR 7950	20:47:40.55	−09:29:44.7	3.78	A1 V
BD+28d4211	21:51:11.07	+28:51:51.8	10.51	Op
BD+25d4655	21:59:42.02	+26:25:58.1	9.76	O
HR 8634	22:41:27.64	+10:49:53.2	3.40	B8 V
Feige110	23:19:58.39	−05:09:55.8	11.82	DOp

Considering that the determination of one atmospheric parameter depends on the values of the other parameters, we iterate the whole recalibration process until all the measurements converge. The results will be presented in a separate paper (Huang et al. 2018, in preparation).

The newly selected 918 template stars consist of two parts. For the first group, we select all stars in PASTEL of effective temperatures higher than 10 000 K or lower than 3000 K, considering the extreme scarcity of such stars in the MILES library. For the second group, all stars of $T_{\rm eff}$ between 3000 and 10 000 K in the MILES library and

in the PASTEL catalogue are grouped into several metallicity bins, as listed in Table 1. Then stars in a given metallicity bin are plotted on a $T_{\rm eff}$–log$g$ diagram with grids of steps of 200 K and 0.25 dex in $T_{\rm eff}$ and log g, respectively. If available, new template stars are then selected from the PASTEL catalogue to ensure that the LEMONY library contains at least one template star in a given grid cell. As an example, Fig. 1 plots stars from the MILES library and from the PASTEL catalogue in the $T_{\rm eff}$–log$g$ plane for the metallicity bin −0.25 ≤ [Fe/H] < −0.15 dex. The new template stars selected from the PASTEL catalogue are also marked. Table 1 lists the numbers of newly selected stars and those in the MILES library for the individual metallicity **bins.** The distributions of all template stars in the LEMONY library in the $T_{\rm eff}$–log$g$ and $T_{\rm eff}$–[Fe/H] planes are presented in Figs 2 and 3, respectively. These figures show that the LEMONY library has a broader parameter space coverage than the MILES and some of the holes apparent in the distribution of the MILES stars are now filled up by the newly selected targets.

2.2 Observations

To extend the wavelength coverage of the template spectra to the far red, the YFOSC long-slit spectrograph mounted on the YNAO 2.4-m telescope is used with a G8 grism to cover the wavelength range 5150–9800 Å. An EEV 2048 × 4068 CCD of 13.5 μm pixel size was used as detector. The G8 grism has a dispersion of 90 Å mm^{-1}, yielding 1.22 Å per pixel at the detector. This set-up was used to collect red spectra of all stars in the LEMONY library. All stars were observed with the YFOSC spectrograph with a slit width of 0.58 arcsec projected on the sky, yielding a FWHM resolution of ∼3.6 Å. Right after the science exposures, exposures of the He–Ne lamp were obtained to wavelength-calibrate the YFOSC spectra.

The blue spectra of the newly added stars are collected with the OMR long-slit spectrograph mounted on the NAOC 2.16-m telescope using a 1200B grating, covering 3800–5180 Å. A SPEC10
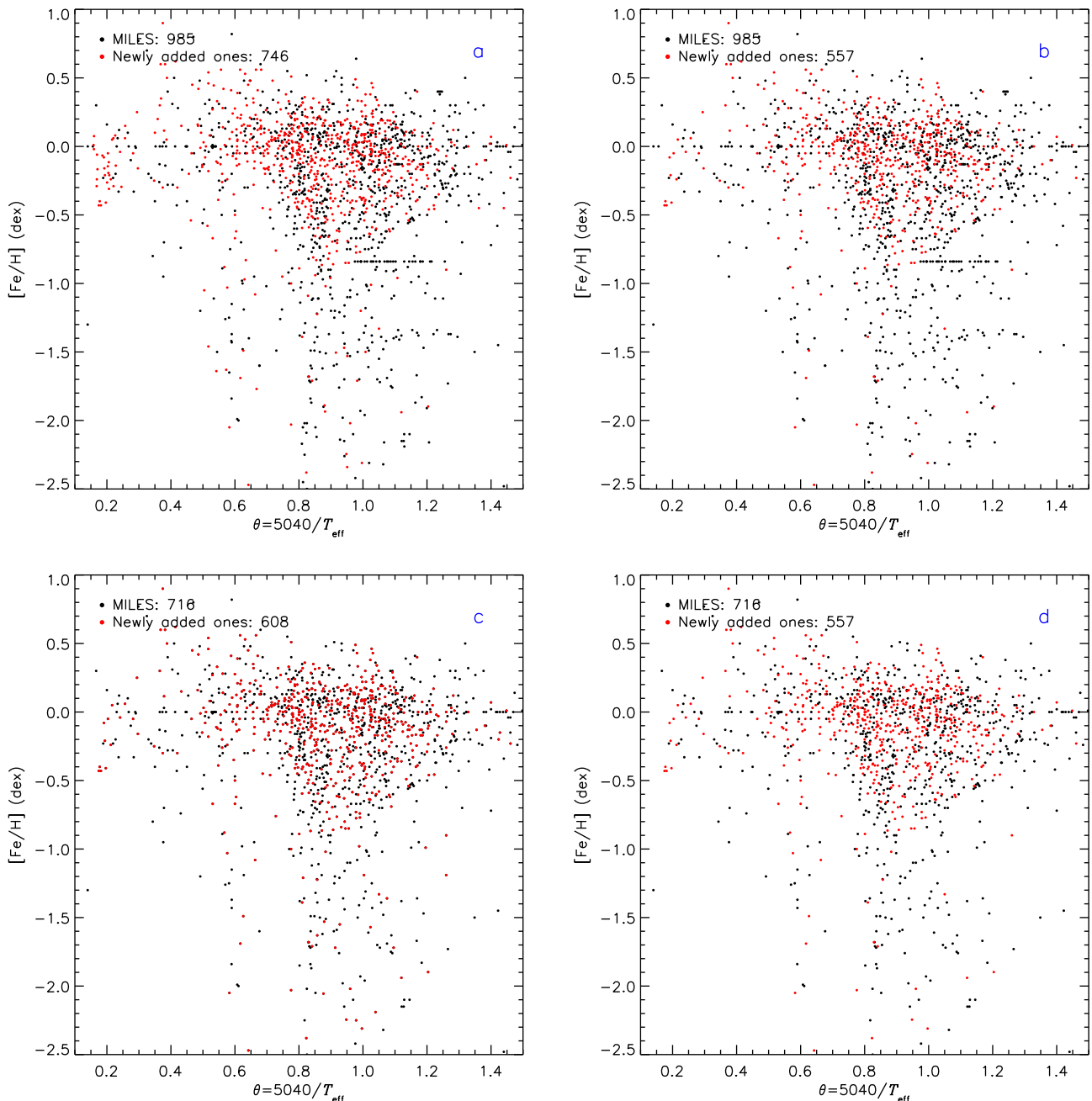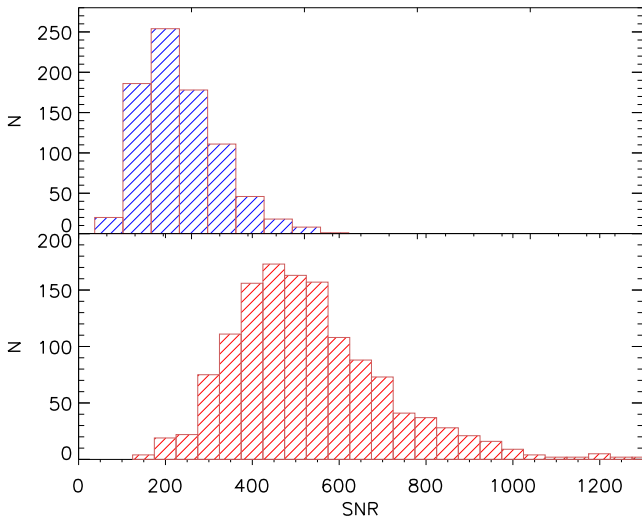
Figure 4. The distributions of stars in the LEMONY library with spectra of different wavelength coverages in the T_{eff}–[Fe/H] plane. Panels a, b, c and d shows stars with spectra covering 3800–5180, 3800–7200, 5150–9000 and 3800–9000 Å, respectively. Black and red dots denote stars from the MILES library and the newly added stars selected from the PASTEL catalogue, respectively.

1340×400 CCD of 20 μm pixel size was used as detector. The 1200B grating has a dispersion of 50 Å mm^{-1}, yielding 1.03 Å per pixel at the detector. A slit width of 1.8 arcsec was used to obtain the blue spectra with a FWHM resolution of ∼2.8 Å. The exposures of the He–Ar lamp were also collected to wavelength-calibrate the OMR spectra.

For the purpose of accurate flux-calibration, all stars were also observed with a wide slit of widths 5.05 and 9.5 arcsec with the YFOSC and OMR spectrographs, respectively. Those same wide slits were used to observe spectral standard stars for the flux-calibration. After flux-calibration, the spectrum of a template star obtained with the narrow slit was scaled with a low-order polynomial function

to match the spectral energy distribution (SED) of the same star obtained with the wide slit.

During the 2013–2017 observational season, 1324 red spectra were collected in 134 (partial) observing nights with the YNAO 2.4-m telescope and 822 blue spectra were obtained in another 58 nights with the NAOC 2.16-m telescope. LEMONY contains 822 blue spectra and 1324 red spectra. Including the spectra of MILES, we now have 1731 stars with spectra covering 3800–5180 Å, 1542 stars with spectra covering 3800–7500 Å, 1324 stars with spectra covering 5150–9000 Å and 1273 stars with spectra covering 3800–9000 Å. Fig. 4 plots the distributions of those four groups of stars in the T_{eff}–[Fe/H] plane. The figure shows that template stars with

Figure 5. Distributions of mean S/N ratios of the LEMONY blue (top) and red (bottom) template spectra.

spectra covering 3800–7500 Å cover a broader parameter space than the MILES stars and some of the holes apparent in the distribution of the MILES stars are now filled up by the newly observed targets. The 1324 stars with YFOSC red spectra also have a broad parameter space coverage. These stars can be used as templates to estimate the atmospheric parameters from the LAMOST red-arm spectra for stars that are either intrinsically red (i.e. of late spectral types) or heavily reddened by the interstellar dust grains. Compared with ELODIE, the 1542 stars with spectra covering 3800–7500 Å contain more metal-poor giant stars.

3 DATA REDUCTION

All LEMONY spectra were reduced with IRAF.[1] The reduction included several steps: bias subtraction, flat-fielding, cosmic ray cleaning, sky background subtraction, one-dimensional spectrum extraction, wavelength-calibration and (relative) flux-calibration. The wavelength-calibration and relative flux-calibration are the essential steps affecting the spectral quality. In the following subsections, we describe these two steps in some detail and the accuracy achieved.

3.1 Spectral S/N ratio and resolution

For the purpose of being used as the template spectra for the derivation of stellar atmospheric parameters from LAMOST spectra, the template spectra should have good S/N ratios and a resolution comparable to that of LAMOST spectra. The mean S/N ratios over the whole wavelength range of almost all our LEMONY spectra are higher than 100, except for 81 blue spectra, but still essentially all higher than 50. The stars with blue spectra of S/N ratios lower than 100 have very low effective temperatures, leading to few photons in blue parts of the spectra. Fig. 5 plots the S/N ratio distributions of the LEMONY blue and red template spectra.
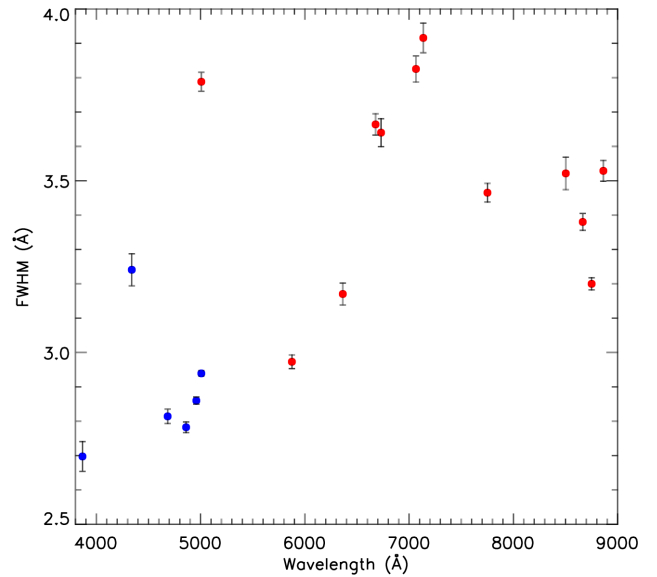
Figure 6. FWHMs of emission lines derived from the blue (blue dots) and red (red dots) spectra of planetary nebulae NGC 2392 and IC 4997 observed with the same instrumental set-ups used for our template stars.

To estimate the spectral resolution as a function of wavelength, we make use of the spectra of planetary nebulae IC 4997 and NGC 2392 obtained with same instruments. The nebulae have rich emission lines across the whole optical spectral wavelength range and expansion velocities much smaller than our spectral resolution. The results are plotted in Fig. 6. As the figure shows, the template spectra have an average resolution FWHM of approximately 2.8, 3.6 and 3.3 Å for the blue, red and the whole spectra, respectively.

3.2 Wavelength-calibration

As mentioned above, the spectra secured with the OMR and YFOSC spectrographs were respectively wavelength-calibrated using He–Ar and He–Ne arc exposures taken after the target observation. The root mean square (rms) residuals of wavelength-calibration were around 0.1 Å. The spectra were then converted to heliocentric wavelengths after being corrected for the diurnal and annual motions of the Earth. By comparing the radial velocities derived from our spectra with LSP3 with those of Gontcharov (2006) (with a mean accuracy of 0.7 km s^{-1}) and Kharchenko et al. (2007) (with a mean accuracy of 2.0 km s^{-1}), we find that the different segments of the spectrum of a given star yield different radial velocities, with a scatter on the level of 20 km s^{-1}, indicating that there are large systematic errors in the spectral dispersion curve deduced from the arc spectrum. The errors are traced back and found to be largely caused by the different light paths and focal lengths between the arc lamp and the celestial target, as well as by the lack of sufficient number of arc lines in the wavelength range λλ5150–5800.

In order to improve the accuracy of wavelength-calibration, we cross-correlate the reduced spectra with theoretical spectra of identical atmospheric parameters. The correlation was carried out for each 250-Å spectral segment in steps of 50 Å. This wavelength length of 250 Å of spectral segments was chosen based on the following considerations: (i) each spectral segment should contain sufficient information to allow a robust estimate of the velocity offset; (ii) a sufficient number of data points are generated, ensuring a robust polynomial fit of the offset as a function of wavelength.
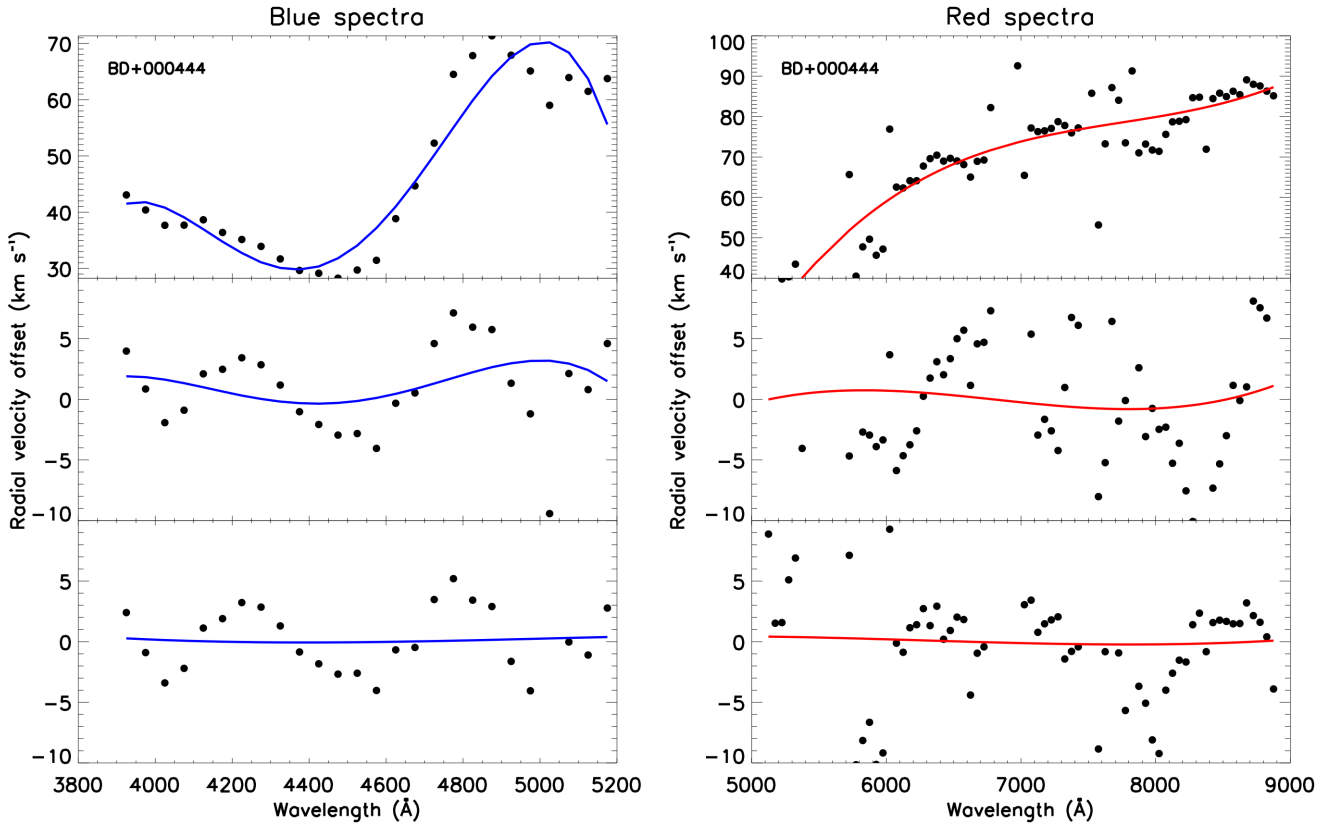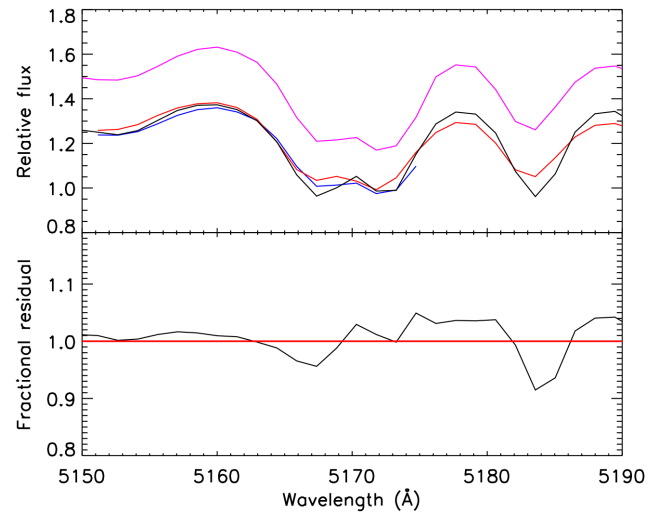
Figure 7. The radial velocity offsets as a function of wavelength for the blue (left panels) and red (right panels) spectra of BD+000444. The top, middle and bottom panels show the results before the corrections and after the first and second rounds of corrections, respectively.
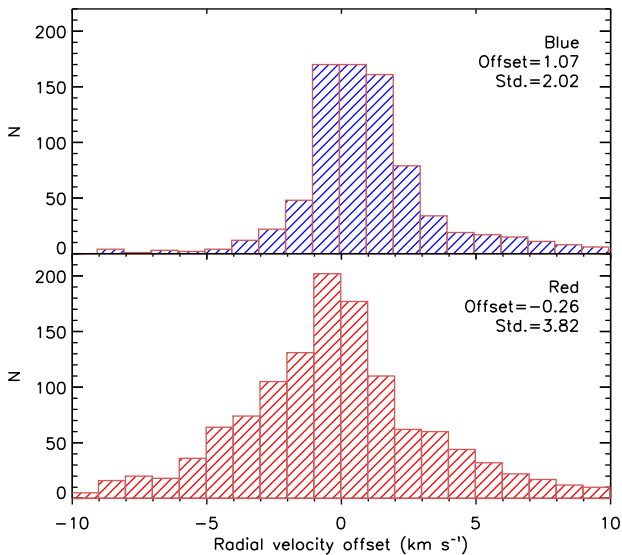
Figure 8. Histograms of radial velocity offsets yielded by the blue (top panel) and red (bottom panel) spectra after correcting for the systematic errors in the spectral dispersion relation deduced from the arc spectrum.

Figure 9. The upper panel shows the MILES spectra (black line), the LEMONY blue (blue line) and red (red line) spectra and the final combined (scaled by a factor of 1.2 for clarity; magenta line) spectra of star HD 054810 in the wavelength range from 5150 to 5190 Å. The fractional differences between the MILES and our combined spectra are plotted in the lower panel. The horizontal red line indicates zero difference.

The theoretical spectra were obtained by interpolating the synthetic spectral library of Munari et al. (2005b) of a spectral resolution $R = 2000$, similar to our observed spectra. The resulting velocity offsets were fitted with a third-order or fourth-order polynomial as a function of wavelength. The fit was then used to correct for errors in the wavelength calibration. This process is repeated twice. Fig. 7 shows

the radial velocity offsets as a function of wavelengths for the blue and red spectra of BD+000444. The top panels show results before the corrections. The middle panels show the results after the first round of corrections. Some systematic variations of the radial veloc-

ity offsets with wavelength remain but are acceptable considering the relatively low resolution of the spectra. The bottom panels show the results after the second round of corrections. The results are similar to those after the first round of corrections, suggesting that the results have converged. For each blue or red spectrum, the coefficients of the polynomial fits are presented in the online catalogues as described in Section 4. After the corrections, radial velocities deduced from the observed spectra with LSP3 show average offsets, after 3σ-clipping, of only -1.07 ± 2.02 and -0.26 ± 3.82 km s^{-1} for the blue and red spectra, respectively, implying a wavelength-calibration accuracy on the level of 4 km s^{-1} (Fig. 8).

3.3 Flux-calibration

For both spectral syntheses of stellar populations and stellar atmospheric parameter determinations, accurate flux-calibration of the SEDs of the template stars is highly desired. For this purpose, several effects need to be considered and corrected for: the instrumental spectral response curve, the wavelength-dependent flux loss for narrow-slit observations due to the atmospheric differential refraction, the atmospheric extinction and the interstellar reddening. To accurately determine the instrumental spectral response curve, each observing night we usually observed three and a minimum of two spectrophotometric standard stars selected from the list available at the ESO website (Oke 1990; Hamuy et al. 1992, 1994). Hot stars with few or weak spectral features were preferred. Table 2 lists the standards used in our observational campaign. As described above, each target was observed with both narrow and wide slits. Spectra obtained with the wide slit were flux-calibrated with the response curve derived from the standards (also observed with the wide slit). The narrow-slit spectra of the targets were then scaled to match the SEDs of the wide-slit spectra. The atmospheric extinction was corrected for using the nominal extinction curve of the site.

The interstellar reddening was corrected for using the reddening law of Fitzpatrick (1999) assuming a total-to-selective extinction ratio $R(V) = 3.1$. Values of selective extinction, i.e. colour excess $E(B - V)$, of all PASTEL stars have been derived by Huang et al. (2018, in preparation) using the 'star pair' technique of Yuan, Liu & Xiang (2013). For stars in the MILES library, the extinction values given in the library were used. Huang et al. (2018, in preparation) have compared values of $E(B - V)$ derived from the 'star pair' technique and those provided in MILES, and found that the differences are mostly smaller than 0.1 mag. The difference is a function of $E(B - V)$ in the sense that the larger the values of $E(B - V)$, the larger the differences. The standard deviation of the differences is about 0.07 mag. Note that for both the purposes of spectral synthesis of stellar populations and stellar atmospheric parameter determinations, accurate relative, rather than absolute, flux-calibration is sufficient.

3.4 Notes

Beyond 7800 Å, the spectra are affected by interference fringing caused by the different light paths between celestial targets and the dome flat on each night, and by the delay of observation of celestial targets relative to the dome flat, which leads to different temperature and thickness of the CCD between the celestial targets and dome flat observations. Typically, the fringing causes fake features with a strength of 5 per cent at the continuous spectrum level, while about 230 of 1324 red spectra are affected by strong interference fringing whose strengths are comparable to that of the absorption lines. The interference fringing was found hardly to be removed
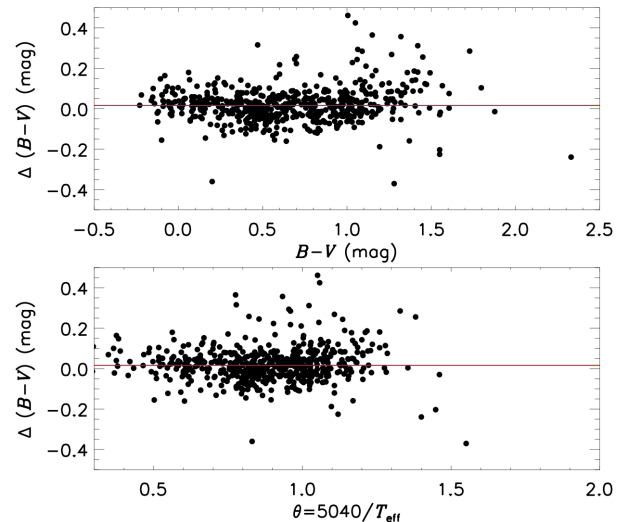
Figure 10. Differences of $B - V$ colours derived from the LEMONY spectra and the photometric values from the Lausanne data base, plotted against the photometric values (top panel) and effective temperature $T_{\rm eff}$ (bottom panel).

from the spectra entirely, and it is a defect of the current data. Stars affected by strong interference fringing are marked by 'flag-f' of value zero, while those unaffected are denoted by 'flag-f' of value one in the catalogues, as described in Section 4.

The red spectra are also affected by a number of strong telluric absorption features, notably the O_2 bands at $\sim$6280 and 6870 Å and the H_2O bands at $\sim$7180, 7800 and 8200 Å. We opt not to rectify those features in our spectra, given the large uncertainties that might be introduced for any correction algorithm. Stars strongly affected by telluric absorption features are marked by 'flag-t' of value zero, and the others by 'flat-t' of value one.

3.5 Combining blue and red spectra

Finally, the blue and red spectra of each star are combined to produce a well flux-calibrated spectrum covering almost the whole optical wavelength range of $\lambda\lambda$3800–9000. The blue spectra are broadened to match the resolution of the red spectra. Given that blue spectra often have a higher S/N ratio and are better calibrated than the red spectra in their overlapping region from 5150 to 5180 Å, the blue spectra are used for the combined spectra. Mg$_1$ and Mg$_2$ lines are located in the overlapping region, and we check their profiles by comparing with the MILES spectra. Fig. 9 shows an example of combining the red and blue spectra for the overlapping wavelength range 5150–5190 Å. The LEMONY and MILES spectra are convolved with Gaussians to a resolution of FWHM $\sim$ 3.6 Å in order to achieve the comparison. The Mg$_1$ and Mg$_2$ line profiles given by the MILES spectrum and by our final combined spectrum match quite well, with fractional differences smaller than 10 per cent. As discussed in Section 4.2, the differences of Lick indices deduced are also very small.

4 DATA ACCESS

The spectra are available online for retrieval at http://lamost973.pku.edu.cn/site/data. The spectra are in FITS format. Note that spectra without correcting for the systematic errors in wavelength calibration are also included. Catalogues containing information of the template stars are also provided, again in FITS format. The infor-
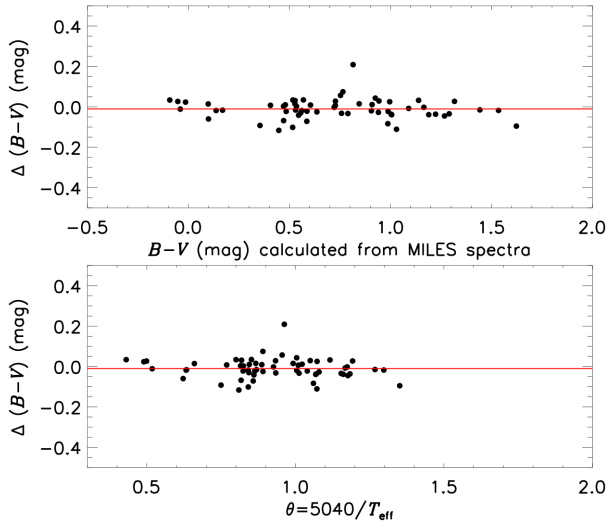
Figure 11. Differences of $B - V$ colours derived from the LEMONY spectra and from MILES spectra for 60 common stars, plotted against the $B - V$ colours calculated from the MILES spectra (top panel) and effective temperature $T_{\rm eff}$ (bottom panel).
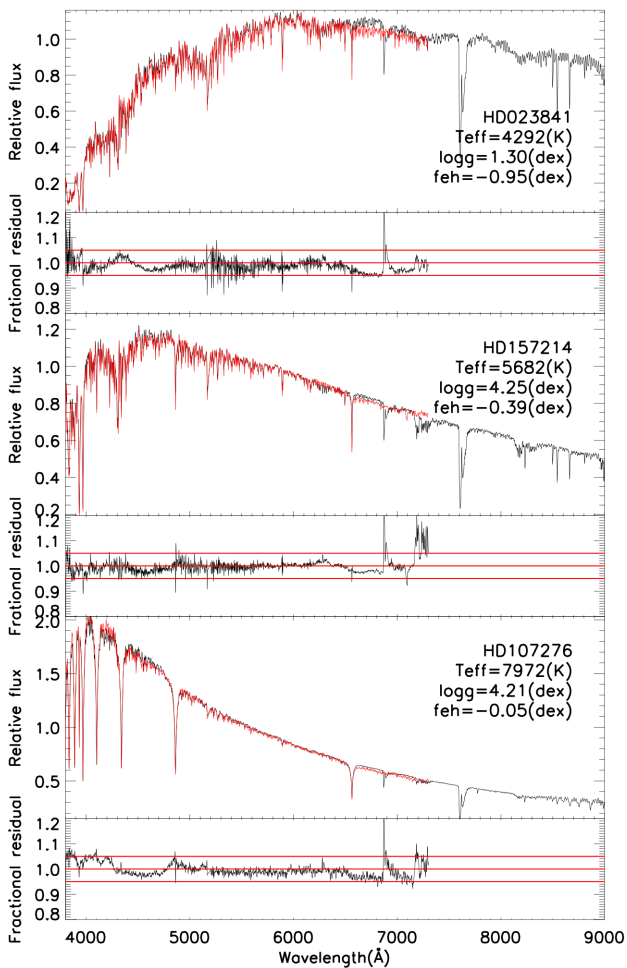
Figure 12. Comparison of the LEMONY spectra (black lines) and those in the MILES library (red lines) for three common targets of different spectral types. The fractional differences are also overplotted at the bottom of each panel. The horizontal lines indicate zero and plus/minus 5 per cent differences, respectively. The star name and atmospheric parameters are marked in each panel.
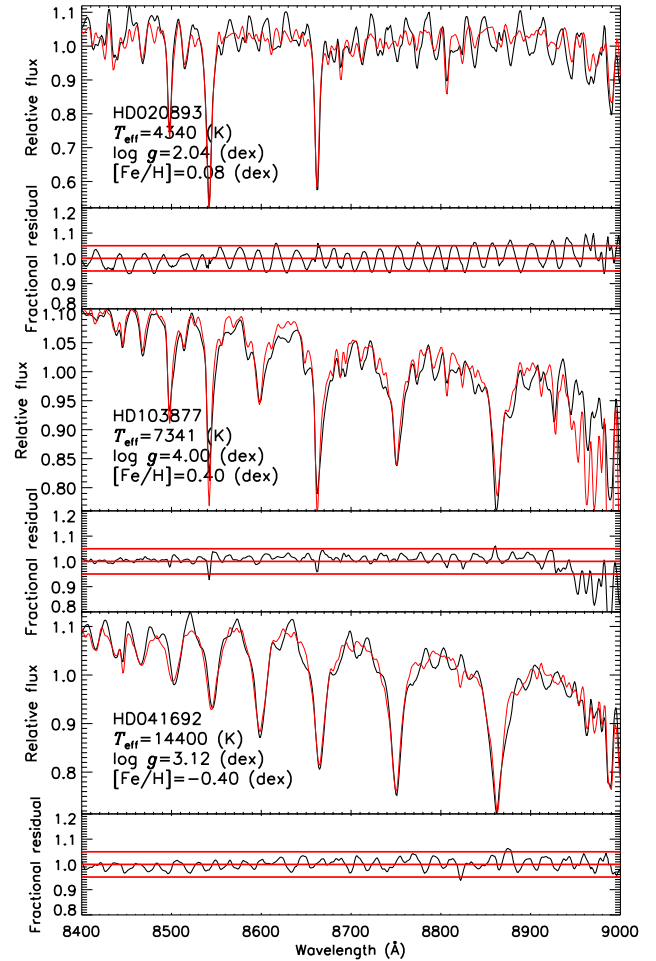
Figure 13. Comparison of our spectra (black lines) and those in the CaT library (red lines) for three common objects of different spectral types. The fractional differences are also overplotted at the bottom of each panel. The horizontal lines indicate zero and plus/minus 5 per cent differences, respectively. The star name and atmospheric parameters are marked in each panel.

mation includes the star name, coordinates, S/N ratios of the blue and red spectra, spectral wavelength range, observational instrument used, observational Julian date, stellar parameters, flags of the spectra and the polynomial fit coefficients used to correct for the systematic errors in wavelength-calibration. A readme file is included with the online data. A detailed description of the catalogue content is presented in Table 3.

5 SPECTRAL QUALITY

In this section, we assess the quality of the LEMONY spectra. In order to examine the SED accuracy, we make two comparisons: (i) a comparison of broad-band colours calculated from our spectra with those calculated from MILES spectra and the photometric measurements in the literature; (ii) a direct comparison between the LEMONY spectra and those in the MILES and CaT (Worthey & Ottaviani 1997) libraries for the common targets in the overlapping spectral regions. To check the strengths of spectral features, we compare the Lick/IDS indices as defined in Worthey & Ottaviani (1997) derived from our spectra with those deduced from the spectra in the MILES and ELODIE libraries for the common targets. We

Table 3. Description of the catalogues.

Name	Description
name	The name of the star
ra	Right ascension of J2000.0 (○)
dec	Declination of J2000.0 (○)
S/N ratio-B	Mean S/N ratio per pixel of blue spectra
S/N ratio-R	Mean S/N ratio per pixel of red spectra
JD-B	Julian date at the middle time of the first exposure of the blue spectra
JD-R	Julian date at the middle time of the first exposure of the red spectra
wavelength range	The wavelength range available
instruments	The telescope and spectrograph used when observing the star
teff	The effective temperature of the star
logg	The surface gravity of the star
feh	The iron-to-hydrogen abundance ratio of the star
ebv	The adopted $E(B - V)$
a1-B	The zero-order coefficient of the polynomial fits of velocity offsets as a function of wavelength for the blue spectra for the first time correction
a2-B	The first-order coefficient of the polynomial fitts of velocity offsets as a function of wavelength for the blue spectra for the first time correction
a3-B	The second-order coefficient of the polynomial fits of velocity offsets as a function of wavelength for the blue spectra for the first time correction
a4-B	The third-order coefficient of the polynomial fits of velocity offsets as a function of wavelength for the blue spectra for the first time correction
a5-B	The fourth-order coefficient of the polynomial fits of velocity offsets as a function of wavelength for the blue spectra for the first time correction
b1-B	The zero-order coefficient of the polynomial fits of velocity offsets as a function of wavelength for the blue spectra for the second time correction
b2-B	The first-order coefficient of the polynomial fits of velocity offsets as a function of wavelength for the blue spectra for the second time correction
b3-B	The second-order coefficient of the polynomial fits of velocity offsets as a function of wavelength for the blue spectra for the second time correction
b4-B	The third-order coefficient of the polynomial fits of velocity offsets as a function of wavelength for the blue spectra for the second time correction
b5-B	The fourth-order coefficient of the polynomial fits of velocity offsets as a function of wavelength for the blue spectra for the second time correction
a1-R	The zero-order coefficient of the polynomial fits of velocity offsets as a function of wavelength for the red spectra for the first time correction
a2-R	The first-order coefficient of the polynomial fits of velocity offsets as a function of wavelength for the red spectra for the first time correction
a3-R	The second-order coefficient of the polynomial fits of velocity offsets as a function of wavelength for the red spectra for the first time correction
a4-R	The third-order coefficient of the polynomial fits of velocity offsets as a function of wavelength for the red spectra for the first time correction
b1-R	The zero-order coefficient of the polynomial fits of velocity offsets as a function of wavelength for the red spectra for the second time correction
b2-R	The first-order coefficient of the polynomial fits of velocity offsets as a function of wavelength for the red spectra for the second time correction
b3-R	The second-order coefficient of the polynomial fits of velocity offsets as a function of wavelength for the red spectra for the second time correction
b4-R	The third-order coefficient of the polynomial fits of velocity offsets as a function of wavelength for the red spectra for the second time correction
flag-s [a]	Mark the observational status
flag-f [b]	Mark whether the red spectrum is strongly affected by interference fringing
flag-t [c]	Mark whether the red spectrum is strongly affected by telluric absorption
flag-v [d]	Mark whether the star is a variable star

[a] flag-s marks the observational status: 0 means that the star only has blue spectrum, 1 means that the star only has red spectrum and 2 means that the star has both blue and red spectra.

[b] flag-f marks whether the red spectrum is strongly affected by interference fringing: 0 means that the red spectrum is strongly affected by interference fringing and 1 means that the effects of interference fringing on the red spectrum are negligible.

[c] flag-t marks whether the red spectrum is strongly affected by telluric absorption: 0 means that the red spectrum is strongly affected by telluric absorption and 1 means that the effects of telluric absorption on the red spectrum are negligible.

[d] flag-v marks whether the star is a variable star: 'y' means that the star is a variable star and 'n' means that the star is not a variable star.

also compare the values of a new set of the near-infrared indices (CaT⋆, CaT and PaT) defined by Cenarro et al. (2001) deduced from our spectra and CaT spectra for the common objects. Table 4 summarizes the information of the three libraries used for the above

Table 4. Spectral libraries used in comparison with our LEMONY spectra.

Library	Wavelength coverage (Å)	FWHM resolution (Å)	Number of stars	Comments
MILES	3525–7500	2.5	985	Long-slit spectra with good flux-calibration
ELODIE	4100–6800	0.5	1347	Echelle spectra
CaT	8348–9020	1.5	706	Long-slit spectra with good flux-calibration

comparisons. The spectra from all the libraries are broadened to match the poorest spectral resolution (average resolution FWHM of ∼3.6 Å for the LEMONY red spectra) of these libraries, and binned to a common linear dispersion of 1.0 Å pixel^{-1}.

5.1 SEDs

From the 628 combined observed spectra (without the interstellar reddening corrections), we calculate the values of broad-band colour $B - V$ using the filter transmission curves of Johnson & Morgan (1953). The results are compared with values taken from the Lausanne photometric data base (Mermilliod, Weidmann & Hauck 1996). The results are shown in Fig. 10. The differences are essentially smaller than 0.2 mag. Some red stars (with large values of $B - V$) have differences larger than 0.3 mag, but the relative differences remain small. The average difference is 0.016 ± 0.07 mag. The small offset sets an upper limit on the systematic uncertainties of our spectral flux-calibration for the spectral range up to ∼ 6000 Å. The standard deviation of the difference is of 0.07 mag. For the 60 common targets, we compare the values of broad-band colours calculated from the combined observed spectra and from the MILES spectra. The results are shown in Fig. 11. The differences are essentially smaller than 0.1 mag with one star of a difference ∼ 0.2 mag. The average difference is −0.01 mag, with a standard deviation of 0.043 mag. Both comparisons suggest an accuracy of relative flux-calibration of a few per cent.

In Fig. 12, we make a direct comparison of our spectra with those from the MILES library for three common targets. In all cases, the fractional differences have a mean and a standard deviation ranging from 1 to 4 per cent. Fig. 13 compares our spectra with those from the CaT library for three common objects for the common wavelength range 8400–9000 Å. Again the agreement is very good, with fractional differences of just a few per cent. Considering the uncertainties of flux-calibration of the MILES and CaT spectra, the telluric absorption features as well as the CCD interference fringing in the far red spectra, the comparisons shown in Figs 12 and 13 indicate that our relative flux-calibration is likely to be much better than 5 per cent.

The standard deviations of fractional differences from three comparisons are also calculated: (i) a comparison between our blue spectra and those from the MILES library for 63 common targets for the common wavelength range $\lambda\lambda 3800$–5150; (ii) a comparison between our red spectra and those from the MILES library for 667 common targets for the common wavelength range $\lambda\lambda 5200$–7400; (iii) a comparison between our red spectra and those from the CaT library for 296 common stars for the common wavelength range $\lambda\lambda 8400$–9000. Fig. 14 shows the standard deviation distributions of the three comparisons. In all comparisons, the fractional differences are calculated by dividing the LEMONY spectra and the MILES library or the CaT library. The resultant fractional standard deviations are essentially all smaller than 10 per cent.

In conclusion, the relative flux-calibration of the spectra in the LEMONY library is likely to be better than 5 per cent.
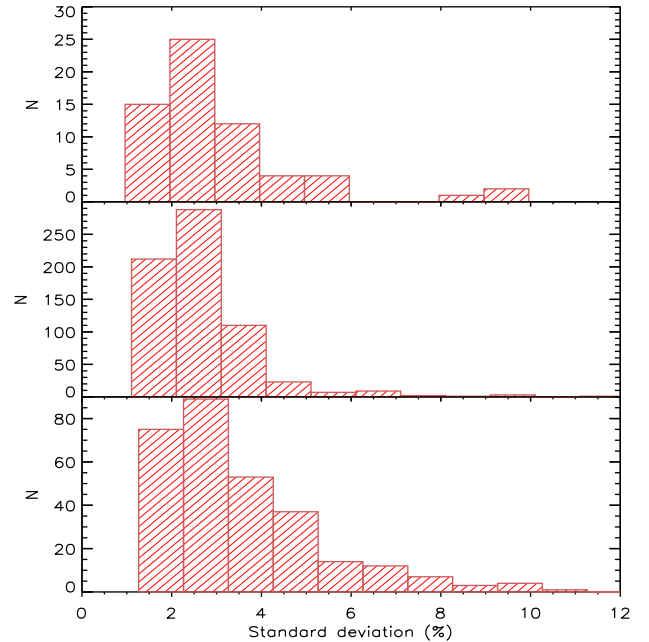
Figure 14. Distributions of standard deviations of fractional differences, after 3σ-clipping, of our blue (top panel) and red (middle panel) spectra and those from the MILES library, and of our red spectra and those from the CaT library (bottom panel).

5.2 Lick/IDS and the near-IR indices

The Lick/IDS indices are derived from the LEMONY spectra and from spectra in the MILES and ELODIE libraries for common objects. The results are compared in Figs 15 and 16. The near-infrared indices are derived from the LEMONY spectra and from those in the CaT library for common stars. Fig. 17 presents a comparison between the near-infrared indices derived from the LEMONY spectra and those deduced from spectra in the CaT library for common stars. The agreement is very good in all cases. There are several stars that show large differences in Lick/IDS indices Fe5270, Fe5335, TiO$_1$ and TiO$_2$. We find that almost all of them are variable stars including two S stars (many of them are long-period variable stars). Linear fits for the individual indices compared are also overplotted in the three figures. The slopes (a) and intercepts (b) of the individual linear fits are also marked in the panels. The values of the slope, intercept and rms of residuals are also listed in Table 5. As the table shows, all slopes have a value close to unity, except when compared with the CaT library, where the slopes are always smaller than 1, implying some systematic differences. The interferometric fringing remaining in the LEMONY spectra may be partly responsible for these differences. The small non-zero intercepts seen in some indices also suggest the presence of some systematic differences between the libraries.
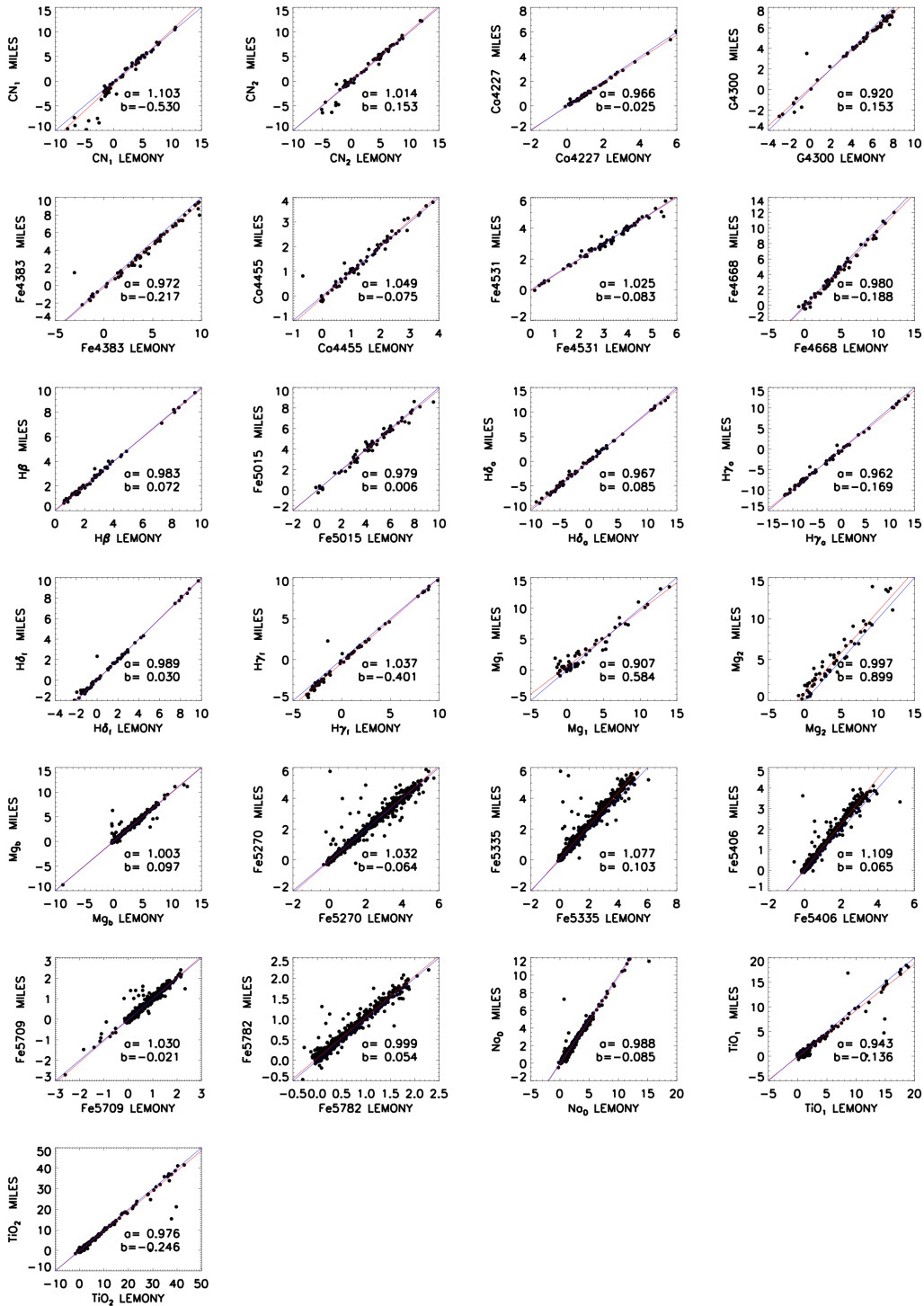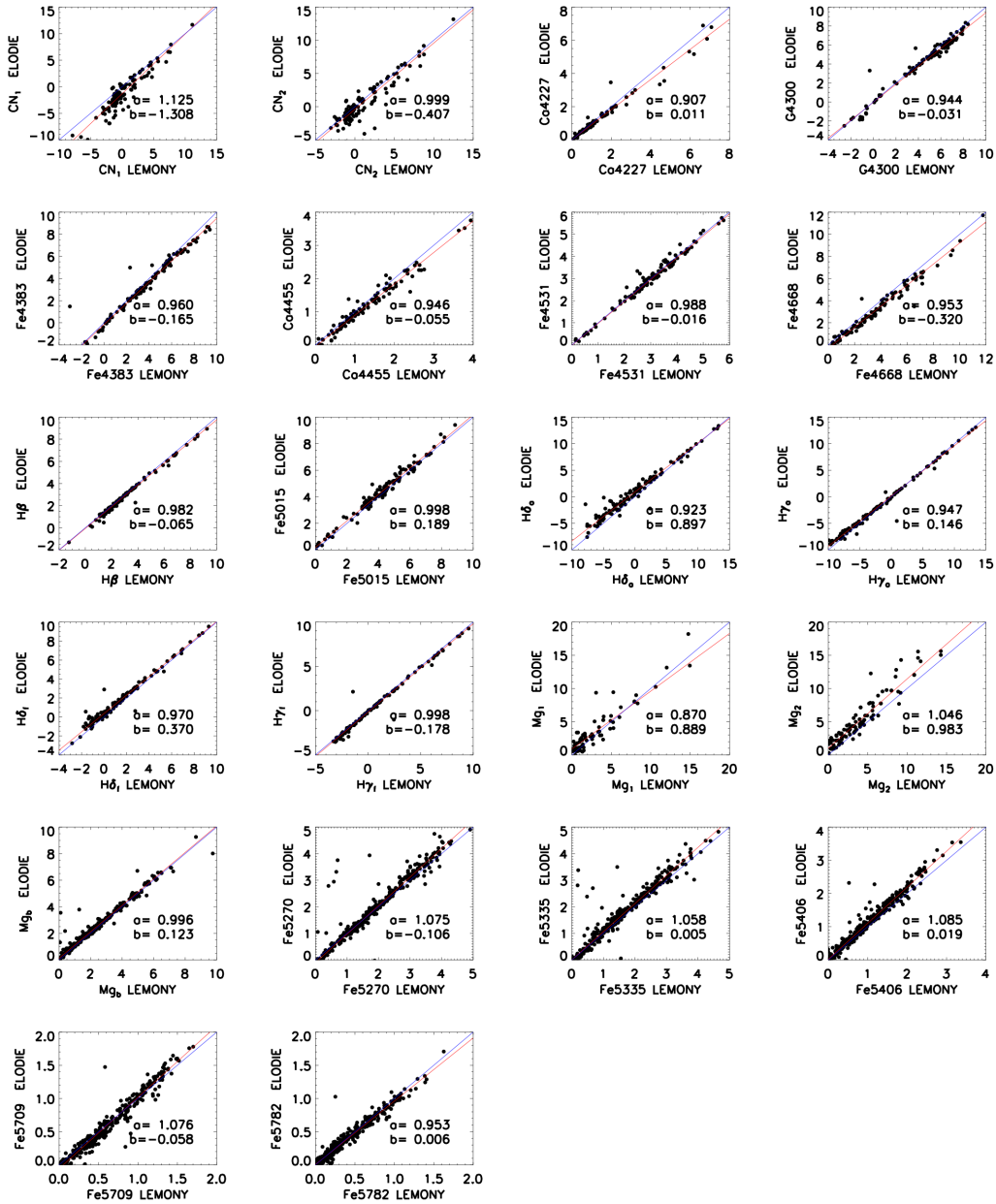
Figure 15. Comparison of Lick/IDS indices derived from spectra in the MILES library and from the LEMONY spectra. The red and blue lines in each panel denote a linear fit to the data and an identity line, respectively. The slope (*a*) and intercept (*b*) of the fit are marked in each panel.

6 IMPROVEMENTS FOR LSP3 USING THE LEMONY LIBRARY

The LEMONY spectra will be added to the empirical template spectral library that LSP3 uses to estimate stellar atmospheric parameters from the LAMOST spectra by template matching. We expect that this will improve LSP3 in at least two ways. First, the new spectra will expand the coverage and improve the homogeneity of the distribution of the MILES template stars in the parameter space, reducing the systematic errors in the derived stellar atmospheric parameters. Second, the 1324 LEMONY red spectra can be used as templates to estimate stellar atmospheric parameters from the LAMOST red-arm spectra. There are ~30 per cent LAMOST spectra having a S/N ratio better than 10 in the red but much worse in blue. For these stars, their stellar atmospheric parameters are expected to be

Figure 16. Same as Fig. 15, but for a comparison of Lick/IDS indices derived from spectra in the ELODIE library and from the LEMONY spectra.
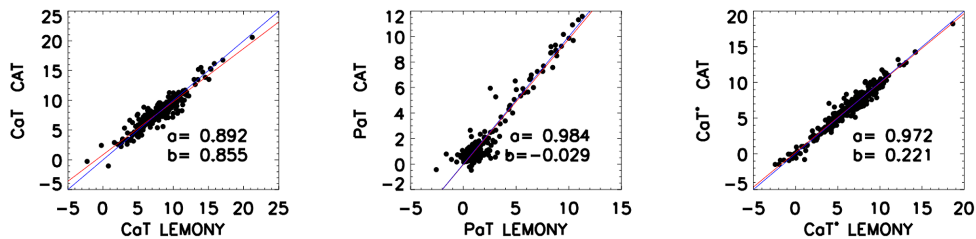
Figure 17. Same as Fig. 15, but for a comparison of the near-infrared indices derived from spectra in the CaT library and from the LEMONY spectra.

determined using the LAMOST red-arm spectra. To test this, we have carried out a simple test to validate the feasibility of deriving stellar atmospheric parameters using the LAMOST red-arm spectra by template matching with our red spectra.

We estimate the atmospheric stellar parameters using spectral segments of wavelength range $\lambda\lambda5800$–9000 with a machine learning method based on Kernel-based principle component analysis (KPCA), as described in Xiang et al. (2017). We select stars of

Table 5. Comparisons of Lick/IDS and the near-infrared indices deduced from our spectra and from spectra in the MILES library and in the ELODIE and CaT libraries. For each data set, the first two columns list the slopes and intercepts of straight-line fits to the data plotted in Figs 15, 16 and 17.

	MILES			ELODIE			CAT		
	Slope	Intercept	rms	Slope	Intercept	rms	Slope	Intercept	rms
CN_1	1.103	−0.530	0.527	1.125	−1.308	1.106			
CN_2	1.014	0.153	0.351	0.999	−0.407	0.981			
Ca4227	0.966	−0.025	0.066	0.907	0.011	0.062			
G4300	0.920	0.153	0.133	0.944	−0.031	0.275			
Fe4383	0.972	−0.217	0.205	0.960	−0.165	0.197			
Ca4455	1.049	−0.075	0.115	0.946	−0.055	0.109			
Fe4531	1.025	−0.083	0.143	0.988	−0.016	0.117			
Fe4668	0.980	−0.188	0.356	0.953	−0.320	0.271			
Hβ	0.983	0.072	0.119	0.982	−0.065	0.105			
Fe5015	0.979	0.006	0.308	0.998	0.189	0.269			
Hδ_a	0.967	0.085	0.284	0.923	0.897	0.596			
Hγ_a	0.962	−0.169	0.276	0.947	0.146	0.254			
Hδ_f	0.989	0.030	0.109	0.970	0.370	0.223			
Hγ_f	1.037	−0.401	0.183	0.998	−0.178	0.110			
Mg_1	0.907	0.584	0.899	0.870	0.889	0.901			
Mg_2	0.997	0.899	0.917	1.046	0.983	1.002			
Mg_b	1.003	0.097	0.145	0.996	0.123	0.128			
Fe5270	1.032	−0.064	0.146	1.075	−0.106	0.118			
Fe5335	1.077	0.103	0.171	1.058	0.005	0.142			
Fe5406	1.109	0.065	0.105	1.085	0.019	0.099			
Fe5709	1.030	−0.021	0.087	1.076	−0.058	0.073			
Fe5782	0.999	0.054	0.074	0.953	0.006	0.055			
Na5849	0.988	−0.085	0.180						
TiO_1	0.943	−0.136	0.327						
TiO_2	0.976	−0.246	0.371						
CaT							0.892	0.855	0.867
PaT							0.984	−0.029	0.568
CaT∗							0.972	0.221	0.648

$3000 \leq T_{\rm eff} \leq 8500$ K, [Fe/H] $\geq −3.5$ dex and $\log g \geq 0$ dex in the LEMONY library as the training set, which contains 1156 stars in total. We adopt 100 principle components (PCs) in fitting the atmospheric parameters with a multidimensional linear function. The residuals of the fits are shown in Fig. 18, which shows that the residuals of atmospheric parameters of 95 per cent of the total 1156 stars are within three standard deviations from a mean. The residuals have a dispersion of 139 K, 0.34 dex and 0.19 dex for $T_{\rm eff}$, $\log g$ and [Fe/H] after 3σ-clipping, respectively.

In order to examine whether the small dispersions of residuals are caused by overfitting, we have carried out an analysis with the so-called leave-one-out approach. We select one star as the test sample, the other remaining 1155 stars as the training set, and we then estimate the atmospheric parameters of the test star. The exercise is repeated 1156 times, each time with a different test star. Fig. 19 shows a comparison of the atmospheric parameters thus deduced with the KPCA method and those from PASTEL catalogue. Again the figure shows that the residuals of atmospheric parameters of 95 per cent of the total 1156 stars are within three standard deviations from a mean. The differences in $T_{\rm eff}$, $\log g$ and [Fe/H] are $−9 \pm 148$ K, 0.00 ± 0.37 dex and $−0.02 \pm 0.21$ dex after 3σ-clipping, respectively. The dispersions are thus comparable to those of the fitting residuals of the training set shown in Fig. 18. The exercise eliminates the possibility that we have significantly overfitted the data.

We have also estimated the atmospheric parameters with the leave-one-out approach using the spectral segments of wavelength range $\lambda\lambda 5800$–7400 of the 763 MILES spectra. Fig. 20 shows a comparison of the atmospheric parameters deduced with the KPCA method and those from the MILES library. The figure shows that the

residuals of atmospheric parameters of only 77 per cent of the total 763 stars are within three standard deviations from a mean. The differences in $T_{\rm eff}$, $\log g$ and [Fe/H] are $−3 \pm 145$ K, $−0.02 \pm 0.43$ dex and $−0.01 \pm 0.23$ dex after 3σ-clipping, respectively. The dispersion of differences in $\log g$ is much larger than that derived using the LEMONY red spectra as the templates.

In conclusion, when deriving the stellar atmospheric parameters using the LAMOST red-arm spectra, template matching with the LEMONY red spectra yields **much better** results than template matching with the MILES spectra. However, more tests of the method are needed before applying it to the whole LAMOST data set, considering most of the LAMOST spectra have much lower S/N ratios than those of the template stars.

7 SUMMARY

In this work, we built a new stellar spectral library, LEMONY, based on observations using the OMR long-slit spectrograph mounted on the NAOC 2.16-m telescope and the YFOSC long-slit spectrograph mounted on the YNAO 2.4-m telescope. The coverage in the parameter space is originally based on MILES, but expanded by selecting targets from the PASTEL catalogue in order to improve the coverage and homogeneity of the distribution of the MILES template stars. The wavelength coverage of the template spectra is also extended to the far red beyond the Ca II triplet.

Hitherto, 822 OMR (blue) and 1324 YFOSC (red) spectra, covering wavelength ranges $\lambda\lambda 3800$–5180 and $\lambda\lambda 5150$–9000, respectively, have been observed and reduced. The spectra have a FWHM resolution of about 3.3 Å, and a mean S/N ratio higher than 100 per
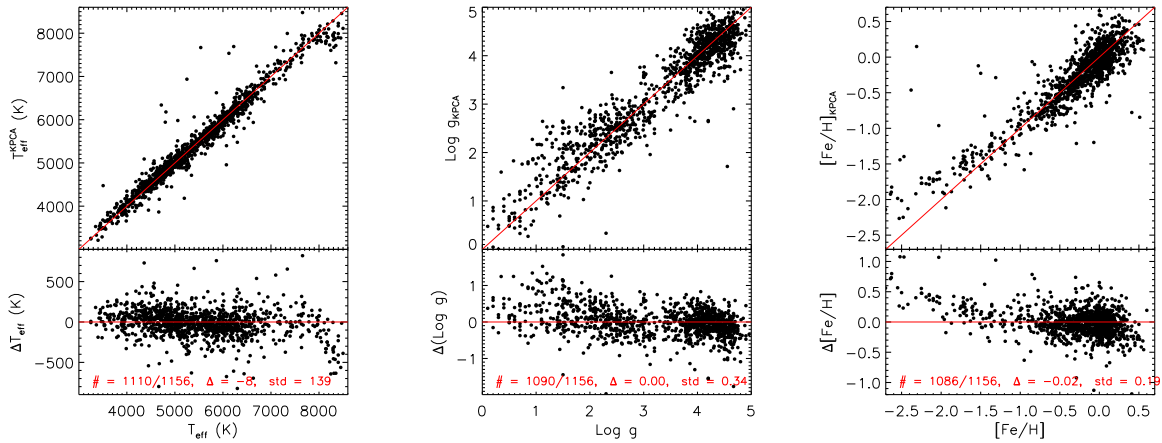
Figure 18. Residuals of the KPCA fits. The upper panels show direct comparisons of parameters given by the fits and those from the PASTEL catalogue, while the lower panels show the residuals. The number of stars after and before 3σ-clipping, the offset and dispersion of the residuals are marked in the lower panel for each compared parameter. The red lines in the top and bottom panels represent the identity lines and zero parameter differences, respectively.
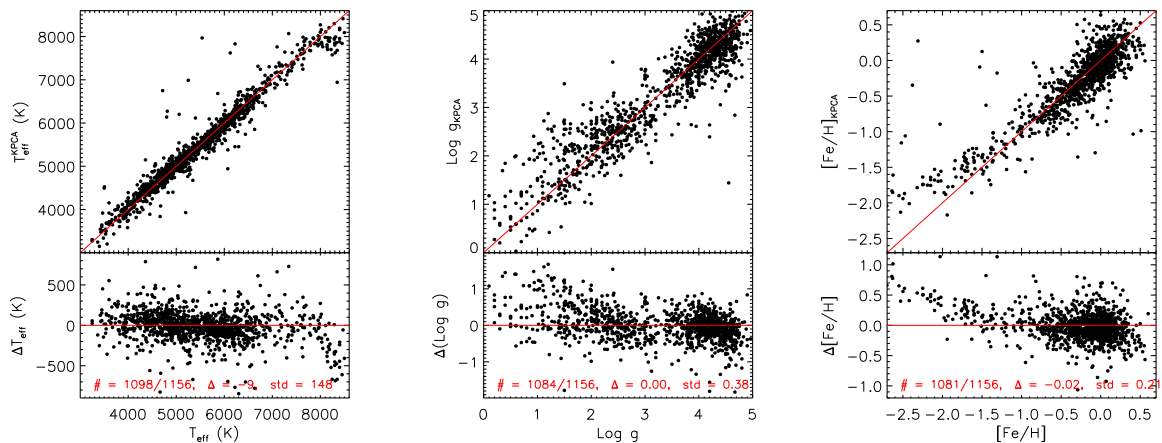
Figure 19. Same as Fig. 18, but for comparisons of atmospheric parameters deduced with the KPCA method (adopting the leave-one-out approach) and those from the PASTEL catalogue. The red lines in the top and bottom panels represent the identity lines and zero parameter differences, respectively.
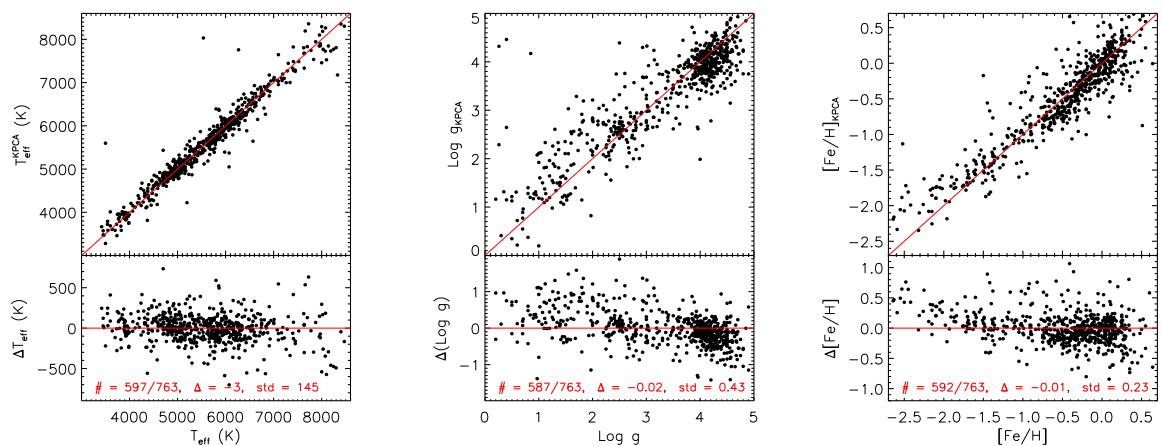
Figure 20. Same as Fig. 19, but for comparisons of atmospheric parameters deduced using the MILES spectra as templates.

pixel for essentially all of them. Accuracies of ~0.3 Å and ~5 per cent have been achieved for the wavelength- and flux-calibration, respectively. The wavelength-calibration is further improved to an accuracy of ~ 4 km s^{-1} after correction for the systematic errors in the spectral dispersion relations derived from the arc spectra.

Comparison of broad-band $(B - V)$ colours calculated from the LEMONY spectra with those calculated from the MILES spectra and the photometric measurements from the Lausanne photometric data base, and comparison between the LEMONY spectra with those from the MILES and CaT libraries for the common stars,

all suggest a relative flux-calibration accuracy of the LEMONY spectra of ~ 5 per cent. The Lick/IDS and the near-infrared indices derived from the LEMONY spectra are also consistent with those derived from the spectra in the MILES, ELODIE and CaT libraries. Currently, the LEMONY library contains 822 blue and 1324 red spectra. Together with the MILES spectra, we now have 1731, 1542, 1324 and 1273 stars with high-quality spectra covering wavelength ranges $\lambda\lambda 3800$–5180, $\lambda\lambda 3800$–7500, $\lambda\lambda 5150$–9000 and $\lambda\lambda 3800$–9000, respectively. Compared with the MILES library, the coverage and homogeneity of the distribution of the template stars in the LEMONY library in the parameter space are much improved. In addition, a significant fraction of the stars have red spectra extending in wavelength beyond the Ca ɪɪ triplet.

The LEMONY library is expected to reduce the systematic errors of atmospheric parameters deduced with LSP3. The 1324 LEMONY red spectra will be used as template spectra to estimate atmospheric parameters from the LAMOST red-arm spectra, for stars either intrinsically red (i.e. of late spectral types) or heavily reddened by the interstellar dust grains, increasing the number of stars surveyed by LAMOST with atmospheric parameters determined by ~ 30 per cent. The LEMONY library should also be useful for stellar population syntheses of galaxies and clusters in a wide wavelength coverage. Of course, it should also benefit other studies, such as the spectral classification of stars, tests of the stellar atmospheric models,etc.

ACKNOWLEDGEMENTS

REFERENCES

Adelman-McCarthy J. K. et al., 2008, ApJS, 175, 297
Barbuy B., Perrin M.-N., Katz D., Coelho P., Cayrel R., Spite M., Van't Veer-Menneret C., 2003, A&A, 404, 661
Boeche C. et al., 2011, AJ, 142, 193
Bruzual G., Charlot S., 2003, MNRAS, 344, 1000
Buzzoni A., 1989, ApJS, 71, 817
Cenarro A. J., Cardiel N., Gorgas J., Peletier R. F., Vazdekis A., Prada F., 2001, MNRAS, 326, 959
Chen Y-P., Trager S. C., Peletier R. F., Lançon A., Vazdekis A., Prugniel P., Silva D. R., Gonneau A., 2014, A&A, 565, A117
Coelho P., Barbuy B., Meléndez J., Schiavon R. P., Castilho B. V., 2005, A&A, 443, 735
Deng L-C. et al., 2012, Research in Astronomy and Astrophysics, 12, 735
Falcón-Barroso J., Sánchez-Blázquez P., Vazdekis A., Ricciardelli E., Cardiel N., Cenarro A. J., Gorgas J., Peletier R. F., 2011, A&A, 532, A95
Fitzpatrick E. L., 1999, PASP, 111, 63
Gontcharov G. A., 2006, Astron. Lett., 32, 759
Guiderdoni B., Rocca-Volmerange B., 1987, A&A, 186, 1
Hamut M., et al., 1994, PASP, 106, 566
Hamuy M., et al., 1992, PASP, 104, 533
Heap S. R., Lindler D. J., 2007, in Vallenari A., Tantalo R., Portinari L., Moretti A., eds, ASP Conf. Ser. Vol. 374, From Stars to Galaxies: Building the Pieces to Build Up the Universe, Astron. Soc. Pac., San Francisco, p. 409
Huang Y., Liu X-W., Yuan H-B., Xiang M-S., Chen B-Q., Zhang H-W., 2015, MNRAS, 454, 2863
Jofré P. et al., 2015, A&A, 582, A81
Johnson H. L., Morgan W. W., 1953, ApJ, 117, 313
Jones L.-A., 1999, PhD Thesis. Univ. of North Carolina, Chapel Hill
Kharchenko N. V., Scholz R.-D., Piskunov A. E., Roeser S., Schilbach E., 2007, VizieR Online Data Catalog, 3254, 0
Lastennet E., Lejeune T., Oblak E., Westera P., Buser R., 2002, Ap&SS, 280, 83
Le Borgne J.-F. et al., 2003, A&A, 402, 433
Lee Y. S. et al., 2008, AJ, 136, 2022
Leitherer C., Ortiz Otálvaro P. A., Bresolin F., Kudritzki R.-P., Lo Faro B., Pauldrach A. W. A., Pettini M., Rix S. A., 2010, ApJS, 189, 309
Leitherer C. et al., 1996, PASP, 108, 996
Liu X-W., Zhao G., Hou J-L., 2015, Research in Astronomy and Astrophysics, 15, 1089
Liu X-W. et al., 2014, in Feltzing S., Zhao G., Walton N. A., Whitelock P., eds., Proc. IAU Symp. Vol. 298, Setting the scene for Gaia and LAMOST, Kluwer, Dordrecht, p. 310
Luo A-L. et al., 2015, Research in Astronomy and Astrophysics, 15, 1095
Majewski S., 2012, in Chemical Evolution of the Milky Way. p. 24
Martins L. P., Coelho P., 2007, MNRAS, 381, 1329
Martins L. P., González Delgado R. M., Leitherer C., Cerviño M., Hauschildt P., 2005, MNRAS, 358, 49
Mermilliod J.-C., Weidmann N., Hauck B., 1996, Baltic Astronomy, 5, 413
Milone A. d. C., Sansom A., Vazdekis A., Sánchez-Blázquez P., Allende Prieto C., Falcón-Barroso J., da Silva R., 2014, Rev. Mex. Astron. Astrofis. Conf. Ser., 44, 49
Munari U., Sordo R., Castelli F., Zwitter T., 2005a, A&A, 442, 1127
Munari U., Sordo R., Castelli F., Zwitter T., 2005b, A&A, 442, 1127
Murphy T., Meiksin A., 2004, MNRAS, 351, 1430
Oke J. B., 1990, AJ, 99, 1621
Perryman M. A. C. et al., 1997, A&A, 323, L49
Prugniel P., Soubiran C., 2001, A&A, 369, 1048
Röck B., Vazdekis A., Ricciardelli E., Peletier R. F., Knapen J. H., Falcón-Barroso J., 2016, A&A, 589, A73
Soubiran C., Le Campion J.-F., Cayrel de Strobel G., Caillo A., 2010, A&A, 515, A111
Steinmetz M. et al., 2006, AJ, 132, 1645
Sánchez-Blázquez P. et al., 2006, MNRAS, 371, 703
Valdes F., Gupta R., Rose J. A., Singh H. P., Bell D. J., 2004, ApJS, 152, 251
Vazdekis A., 1999, ApJ, 513, 224
Vazdekis A., Ricciardelli E., Cenarro A. J., Rivero-González J. G., Díaz-García L. A., Falcón-Barroso J., 2012, MNRAS, 424, 157
Villaume A., et al., 2017, ApJS, 230, 23
Worthey G., 1994, ApJS, 95, 107
Worthey G., Ottaviani D. L., 1997, ApJS, 111, 377
Wu Y. et al., 2011, Research in Astronomy and Astrophysics, 11, 924
Xiang M-S. et al., 2017, MNRAS, 464, 3657
Xiang M. S. et al., 2015, MNRAS, 448, 822
Yanny B. et al., 2009, AJ, 137, 4377
Yuan H-B. et al., 2015, MNRAS, 448, 855
Yuan H. B., Liu X. W., Xiang M. S., 2013, MNRAS, 430, 2188
Zhao G., Zhao Y-H., Chu Y-Q., Jing Y-P., Deng L-C., 2012, Research in Astronomy and Astrophysics, 12, 723

This paper has been typeset from a TEX/LATEX file prepared by the author.